THERMAL ANALYSIS METHODS FOR AN EARTH ENTRY VEHICLE

Eleventh Thermal and Fluids Analysis Workshop
August 21-25, 2000
Cleveland, Ohio

Ruth M. Amundsen, John A. Dec, Michael C. Lindell
National Aeronautics and Space Administration
Langley Research Center
Hampton VA 23681-2199

THERMAL ANALYSIS METHODS FOR AN EARTH ENTRY VEHICLE

Ruth M. Amundsen, John A. Dec, Michael C. Lindell
National Aeronautics and Space Administration
Langley Research Center
Hampton VA 23681-2199

ABSTRACT

Thermal analysis of a vehicle designed to return samples from another planet, such as the Earth Entry vehicle for the Mars Sample Return mission, presents several unique challenges. The Earth Entry Vehicle (EEV) must contain Martian material samples after they have been collected and protect them from the high heating rates of entry into the Earth's atmosphere. This requirement necessitates inclusion of detailed thermal analysis early in the design of the vehicle. This paper will describe the challenges and solutions for a preliminary thermal analysis of an Earth Entry Vehicle. The aeroheating on the vehicle during entry would be the main driver for the thermal behavior, and is a complex function of time, spatial position on the vehicle, vehicle temperature, and trajectory parameters. Thus, the thermal analysis must be closely tied to the aeroheating analysis in order to make accurate predictions. Also, the thermal analysis must account for the material response of the ablative thermal protection system (TPS). For the exo-atmospheric portion of the mission, the thermal analysis must include the orbital radiation fluxes on the surfaces. The thermal behavior must also be used to predict the structural response of the vehicle (the thermal stress and strains) and whether they remain within the capability of the materials. Thus, the thermal analysis requires ties to the three-dimensional geometry, the aeroheating analysis, the material response analysis, the orbital analysis, and the structural analysis. The goal of this paper is to describe to what degree that has been achieved.

INTRODUCTION

The purpose of the Mars Sample Return Mission is to return a sample of Martian material to Earth so that it may be studied here. In order for the return of the samples to the Earth's surface to be successful, the Earth Entry Vehicle (EEV) must be robust and extremely reliable. Some of the reasoning behind design of the vehicle is discussed in an earlier publication on a similar design.[1] This paper will describe the thermal modeling and design of one possible design of an EEV (CP5.7) of the many designs under evaluation. The design of a Mars Sample Return Earth Entry Vehicle has many unique finite element modeling challenges associated with it, both of a structural and thermal nature. The purpose of the Earth Entry Vehicle is to protect Mars samples from the mechanical and thermal environment encountered during Earth entry and landing, while assuring sample containment. The science requirement on thermal design is that the returned samples will not experience a temperature over 50°C throughout all mission phases. The system requirement is that no component should go outside its survival temperature range during cruise, or outside its operational temperature range during operation.

The EEV expected lifetime of about three years can be separated into several distinct thermal phases. For the most part of three years (phase 1), it would be attached to the spacecraft during the planetary travel and sample collection intervals. Several days before arrival into the Earth's atmosphere, the EEV would be spin-ejected from the spacecraft and begin the exo-atmospheric cruise portion (phase 2) of the journey. The entry into Earth's atmosphere would be the third phase, with aerodynamic heating boundary conditions very different than the first two phases. The fourth phase would be equilibration of the EEV to ambient temperature conditions on the Earth's surface after landing. Only the last three phases are discussed in this paper.

This paper will describe the challenges inherent in this analysis, and the solutions employed. One challenge is keeping up with rapid design changes and rapid trajectory changes. In order to be useful, the analysis must be able to respond with quick answers to "what-if" scenarios regarding geometry or trajectory changes. Another challenge is defining the exterior properties of the vehicle so that appropriate temperatures are maintained both while attached to the spacecraft, and after separation. The cruise after separation is in a hyperbolic orbit, which complicates the simulation. The heat pulse at entry challenges both the mesh density and the thermal solver. The material responses (such as pyrolysis) during the heat pulse must be taken into consideration. Finally, three-dimensional orthotropic properties on these randomly oriented components are a challenge to incorporate.

The thermal analysis results are valuable for several reasons. First, the thermal environment experienced by the returned samples can be predicted, and if not acceptable for science reasons, design modifications can be made. The thermal history of each material in the vehicle design can also be compared to its survival range, to ensure that all designed materials are adequate. The thermal predictions for operational mechanical and electronic components can be used to ensure they remain within their acceptable thermal range. Another use for the thermal predictions is to predict thermal stresses and deflections in the vehicle. The exo-atmospheric phases involve cold temperatures and slow changes, as well as a moderate gradient across the vehicle. The entry phase involves very rapid changes in temperature and gradients across the vehicle. Each thermal case can be used for structural analysis of the vehicle, to determine if unacceptable stresses or deflections are encountered.

DESIGN DESCRIPTION

This particular preliminary design of an EEV is shown in Figure 1. This is a concept called CP5.7, which incorporates a carbon-phenolic ablator. An earlier design concept utilizing a different ablator is described in an earlier publication[2]. This is an on-going design process, and both the design and associated analysis are expected to change. The forebody thermal protection system (TPS) is carbon-phenolic, and the afterbody TPS is SLA-561V. Both materials have substantial heritage in aerospace missions. The substructure is carbon-carbon. The wing foam is a low density but stiff carbon foam. The samples are held within an orbiting sample canister (OS), and the OS is enclosed within a containment vessel (CV). The CV/OS is within an impact sphere filled with energy absorbing material. The entire forebody is covered with a 3-layer multi-layer insulation blanket (MLI) that extends back to the spin-eject ring on the aft side. The spin-eject ring is where the EEV is mounted to the spacecraft via a mechanism that accomplishes separation and spin-up.

During the 4-day exo-atmospheric cruise after separation, the spin stabilized EEV is in a hyperbolic orbit ending at atmospheric entry. The solar angle during this cruise is at roughly 45° off the nose, such that the solar flux falls only on the forebody.

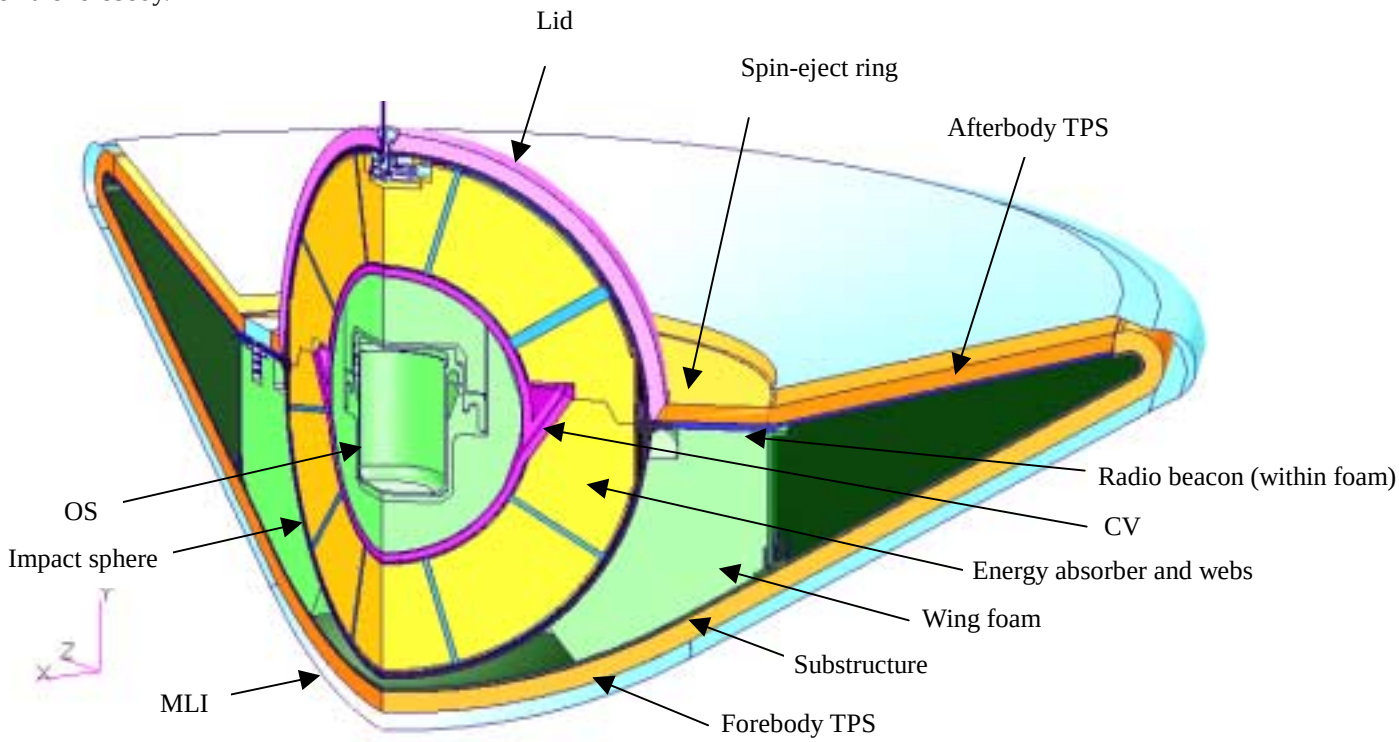

Figure 1. EEV model geometry (120°).

THERMAL MODELING

Geometry

One challenge in modeling an Earth Entry Vehicle (EEV) during preliminary design is tracking frequent design changes. It is important to have an analysis method that allows quick evaluation of potential design modifications. The method employed in this analysis is to import design geometry directly from the computer-aided design (CAD) software Pro/Engineer[3] into the modeling software MSC/PATRAN[4*]. This geometry can be directly meshed to create the analysis model. In some cases, a design modification can be evaluated by simply altering a material or boundary condition in the model. For a more substantial design change, a new geometry or part must be imported. Even when a new geometry is imported, re-analysis can be relatively fast since all the boundary conditions and materials applied to the geometry can be re-used. In this manner, design changes and updates can be rapidly incorporated, rather than necessitating long periods of manual dimension input to the modeling software.

The geometry comes into PATRAN with all parts separated into groups, which facilitates meshing, application of properties and boundary conditions, and model changes. The thermal solver is currently PATRAN Thermal 9.0. The thermal models capture only a portion of the vehicle since it is largely axially symmetric; 120° of the vehicle was modeled to capture non-symmetric items such as body mount bolts, radio beacon, push pads, etc. A previous study evaluated use of a 2D axi-symmetric model. 2D axi-symmetric and 3D partial models were developed, and solved for the same boundary conditions. The 2D axi-symmetric model did not give a faster solution time, and is actually more time-consuming to create from the CAD geometry. Three-dimensional models also allow capturing the behavior of the non-symmetric components. Thus, the 3D models were used for the remainder of the work.

Analysis Methodology

The overall analysis process is shown in Figure 2. Geometry, trajectory, heating and material response information are all incorporated in the PATRAN model. Thermal solution is done with PATRAN Thermal, and temperatures are passed to NASTRAN for structural analysis. Each of these steps will be described in later sections.

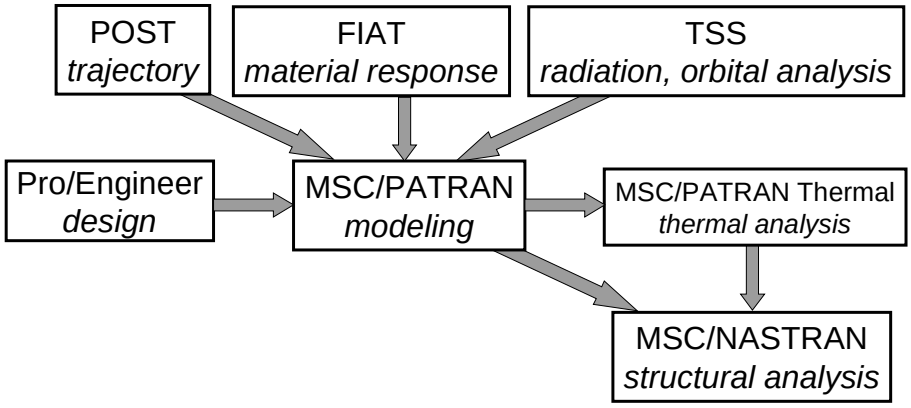

Figure 2. Integrated analysis process.

The modeling is separated into four distinct phases: cruise with the spacecraft, post-separation exo-atmospheric cruise, atmospheric entry to landing, and post-landing. The different phases of analysis have very different timelines and boundary conditions, as well as different requirements for integrating with other analysis. The exo-atmospheric cruise portion may last for several days, and it must include the effects of orbital radiation fluxes. The heat pulse at entry is less than a minute, the entire descent is less than seven minutes, and this model must include aerodynamic heating and material response. Each of these phases must be integrated with structural analysis in order to determine the structural behavior in each phase.

---

[*] The use of trademarks or names of manufacturers in this report is for accurate reporting and does not constitute an official endorsement, either expressed or implied, of such products or manufacturers by the National Aeronautics and Space Administration.

The exo-atmospheric cruise phase and the entry phase have similar boundary conditions in that both have heat fluxes, convection and radiation applied to the entire exterior of the vehicle. However, in the entry phase the heat pulse is severe enough that a very fine mesh must be used. This model is a transient that only lasts for 360 seconds, so the solution time can be kept reasonable even with a very fine mesh. If that dense a mesh were used on the exo-atmospheric case, where the transient is four days and there are many parametric cases to be run, solution time would be excessive. Thus, the same geometry and materials are shared between these two models, but the meshing is different. Temperatures are transferred between the model phases by mapping the results back to the geometry, independent of the differing meshes.

The post-landing model is very similar to the exo-atmospheric case in that it is a long-term transient (24 hours) where a coarse mesh is acceptable. Thus, the same geometry and mesh as the exo-atmospheric case are used, although most boundary conditions are different. The post-landing state of the vehicle presents a challenge since there are many possible alternatives. The vehicle may be in any one of many possible orientations, yielding a host of potential air convection and ground contact possibilities. The range of possible ground material compliance is wide, which can vary the amount of the vehicle in contact with the ground. Also, the time interval before the vehicle is located is variable, and the ambient temperature and wind conditions are difficult to predict. Thus, several general cases must be run to bound the problem.

Model Development

After import from Pro/Engineer, the model consists of trimmed solids. These are a type of solid that can be automatically meshed using tetrahedral (tet) elements in PATRAN, but cannot be automatically meshed with brick (6-sided) elements. Tetrahedral meshes were sufficient for the exo-atmospheric and landed models, since the heating levels were benign enough at the surface to allow a converged solution using tet elements. For these models the imported solids were meshed directly, leading to roughly 50,000 nodes. The exo-atmospheric model is shown in Figure 3 and Figure 4.

The entry model cannot use tet elements on the exterior surfaces. The heating levels drive the tet elements unstable and convergence cannot be achieved without extremely small elements. Also, meshing with tet elements does not allow the charring of the surface to be modeled in successive regular layers with a controlled depth. In order to mesh this model with appropriate bricks, quad surface meshes were developed on the open faces and swept through the model to create bricks that were associated to the original geometry. On some of the interior components, thermal change was slow enough to allow direct tet meshes of the solids. The complete model is shown in Figure 5. The total number of nodes in the model is much larger than in the exo-atmospheric model due to the finer mesh -- 350,000 nodes resulted when the interior was meshed with bricks; the brick-tet hybrid mesh yielded 181,000 nodes. The entry model did not include MLI since this is assumed to burn away very early in the descent.

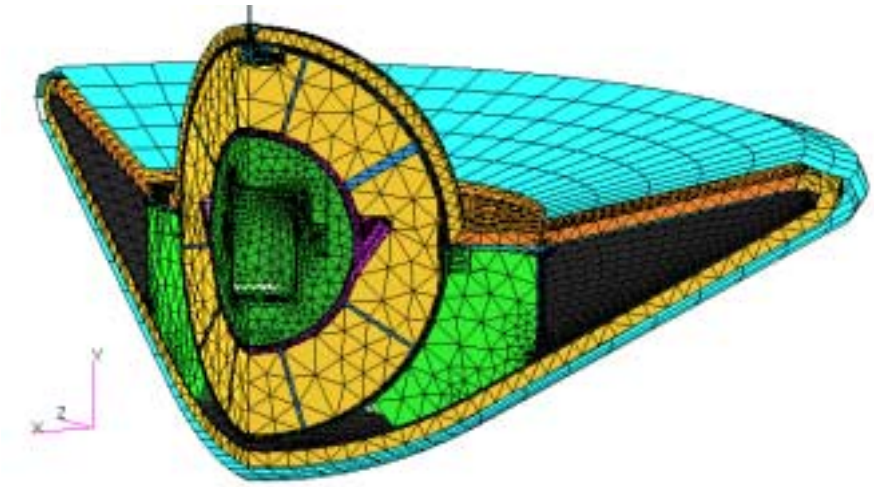

Figure 3. Mesh of exo-atmospheric model.

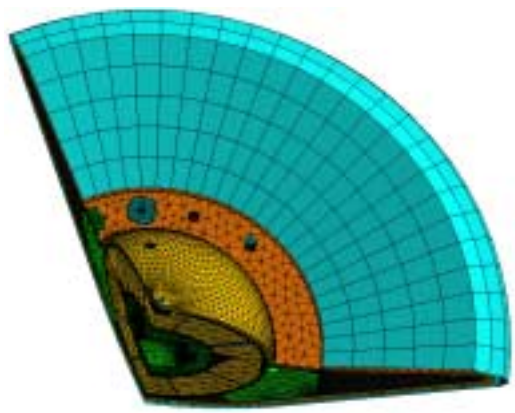

Figure 4. Exo-atmospheric model mesh, showing lid and aftbody penetrations.

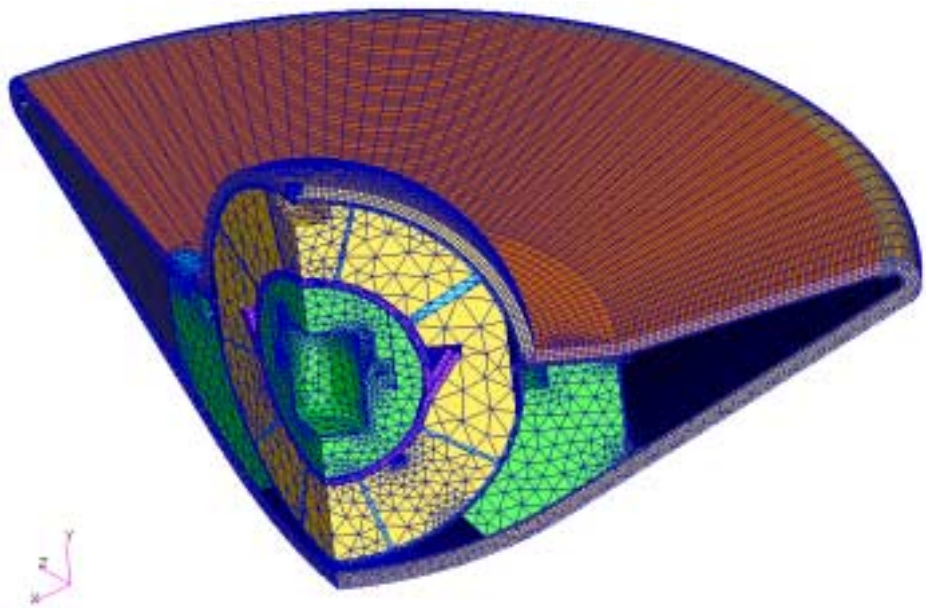

Figure 5. Mesh of entry model.

In both models, boundary conditions and material properties were applied to the geometric entities, rather than to the mesh. Applying boundary conditions to the geometry, rather than the mesh, facilitates both the evaluation of different mesh densities as well as re-meshing when necessary.

Heat Flux Boundary Conditions

A common change that must be anticipated when performing detailed thermal analysis early in the design of the vehicle is modifications to the trajectory and heating rates. When the trajectory changes, both the exo-atmospheric cruise and entry heating loads are affected. Rapid evaluation of the changes is beneficial in allowing final trajectory design. Heat flux boundary conditions are applied via an external text file, so that changes to the trajectory and heating rates can be easily made via substitutions in that file.

Integration with Orbital Analysis

The modeling of orbital fluxes could not be done using PATRAN, so the Thermal Synthesizer System (TSS)[5] software was used. The orbital heat loads during the exo-atmospheric phase must be calculated for a hyperbolic orbit. Many of the available orbital/radiation analysis tools do not handle hyperbolic orbits. TSS was used because of its capability to handle a hyperbolic orbit analysis via input of discrete trajectory points. TSS does not currently have geometry import capability from Pro/Engineer or PATRAN. Thus, this model was developed independently.

This was not a large effort since only the main exterior shapes of the vehicle need to be captured. In order to allow rapid response to design changes, the model was built using variables. By changing one or many of only five variables, the entire outer shape of the vehicle could be modified. This method allowed quick calculation of orbital heating on the exterior of the vehicle, from both solar and planetary sources, for a variety of vehicle shapes, exterior properties and trajectory definitions.

Figure 6 shows an example TSS model with heat fluxes on the vehicle surface, as well as a representation of the final orbit points. Visual verification of the trajectory, orientation and exterior heat fluxes is of significant benefit in the analysis. The vehicle is spinning at 2 rpm, so calculated fluxes were averaged around the vehicle to account for the spin. The averaged fluxes were applied to the PATRAN model as a surface boundary condition. The heat loads from this analysis are automatically captured in a single file, thus simplifying the incorporation of this data into the overall thermal analysis and the evaluation of several trajectories for a single vehicle design.

Since the TSS model is developed independently, this is not a complete analysis integration. However, for this simple exterior, development and modification of the separate model is relatively trivial. Although a tighter integration would be preferable for a more complex model, in this case it is not essential. Future revisions of this process are planned whereby the orbital model will be developed from a STEP* format output of the geometry. Also, the output heat load file format will be modified such that no manual editing is required.

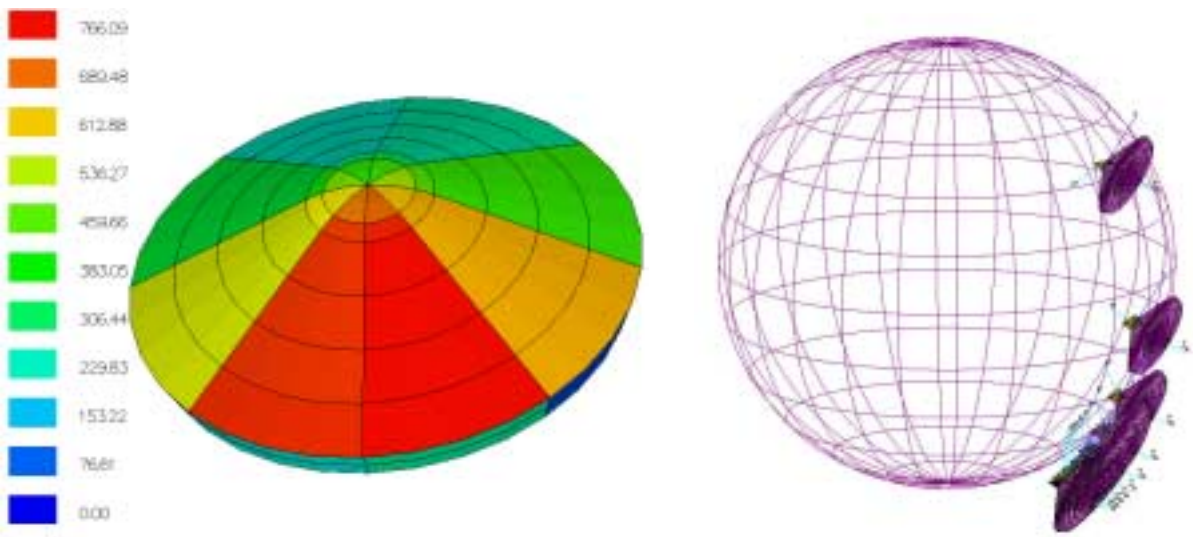

Figure 6. TSS solar flux prediction (W/m2) and trajectory orientation.

Integration with Aeroheating and Material Response

The heat pulse of an earth entry must be modeled precisely in order to fully understand its effect on the subsequent thermal behavior. The aerodynamic heating is a function not only of time, since velocity and atmosphere are both altering radically with time, but also of the position on the vehicle surface. Unique methods were developed to incorporate an accurate representation of this heating into the model.

CFD predictions of heating on the vehicle surface were performed for several discrete time points. In order to have a transient heating profile that includes trajectory effects, the Program to Optimize Simulated Trajectories (POST) code was run. The aerodynamic heating values from this code were corrected using CFD results. This code predicts cold-wall heating values, and does not account for the blocking effect due to ablation and pyrolysis of the TPS material. These material response effects are captured in the Fully Implicit Ablation and Thermal Analysis Program (FIAT)[6] used by NASA Ames for preliminary TPS sizing. FIAT accounts for all of the physical and chemical

---

* Standard for the Exchange of Product Model Data (STEP)

processes occurring in the TPS material**.** The output used from FIAT for this thermal analysis was the hot wall ablative heat flux. This heat flux includes the effects of the actual temperature of the vehicle surface as well as ablation and pyrolysis blocking of heat (blowing factor). This heat flux was used as the input to the PATRAN model. The FIAT analysis is currently only 1D, so several discrete points were used with appropriate spatial factors between them in accordance with the shape of the heating observed in CFD analysis.

These heat flux predictions on the forebody showed gradients both in time and spatial position. To capture this on the forebody, the stagnation point heating (convective plus radiative) as a function of time (Figure 7) was multiplied by the spatial factor on the forebody as function of radial distance (Figure 8). This spatial factor was thus assumed to be constant with time, when it actually changes with time. This will be improved in later modeling, but since the factor is only important over a short time period (about 30 seconds), the approximation is good enough for preliminary design evaluation.

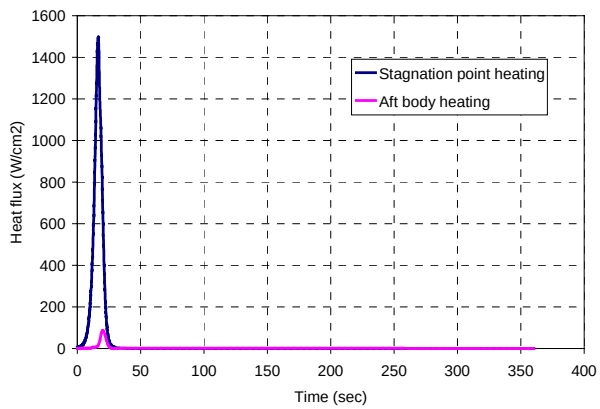

Figure 7. Heat flux versus time on EEV (CP5.7).

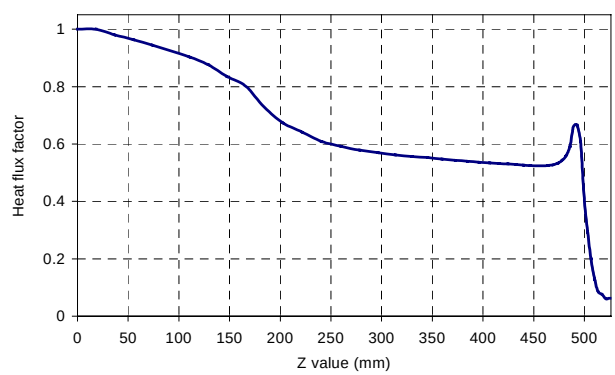

Figure 8. Spatial factor on forebody (CP5.7).

On the afterbody, due to the uncertainty in the spatial variation of afterbody CFD predictions, three points were used for heat flux predictions. The three points were at the aft body stagnation point on the lid, the interior corner where the lid TPS meets the aft TPS, and a point on the shoulder at the max vehicle diameter. Then time-varying spatial factors were developed to interpolate heating between the points. Figure 7 shows the aft body stagnation point flux. Two boundary conditions were created, one between the stagnation point and the interior corner, the other between the shoulder and interior corner. The spatial factors for these boundary conditions were found by dividing the flux at the interior corner by the flux at the stagnation point and flux at the shoulder for each respective set, then interpolating between 1.0 and these ratios. When the flux ratios were plotted over time, they were found to vary. Fortunately, the variations could be separated into three different time intervals in which they were generally constant, and therefore three different spatial fields could be created for each area, and three heat flux boundary conditions could be applied to the lid TPS and aft TPS. To ensure that each boundary condition was active only

during the appropriate time interval, the heat flux boundary conditions were created with unit step-function multipliers to turn them on and off. As an example, the flux applied to the lid TPS was thus the product of the flux at the stagnation point, the spatial factor between the stagnation point and interior corner, and a step function that changed between 1 or 0 based on time.

The heating data when applied in this manner does not account for the charring effects of the ablative TPS materials. In order to correct this, the thermal predictions for TPS sizing at the stagnation point (done by YK Chen at NASA Ames) were used as a baseline for comparison. Several layers of the TPS elements in the model were constructed to include charring as a function of time by changing their properties. By correlating the response of the PATRAN model with the FIAT results, the actual char layer behavior could be corrected such that the PATRAN model shows accurate 3D behavior of the material.

Other Boundary Conditions

Contacts between the components are modeled via pseudo-convection boundary conditions. All components are connected via a 0.25-mm adhesive bond, which gives a contact conductance of 750 W/m^2K. Several parametrics were run with other contact conductances and the variation had little effect. The only unbonded attachment is the OS within the CV; since this is a loose contact connection it is rated at a lower conductance of 100 W/m^2K.

Current assumptions for the exo-atmospheric model include an EEV temperature at release of –80°C. This value is not critical to later operations, since regardless of the release temperature, the EEV will come to the same equilibrium during the four-day cruise before Earth entry. During exo-atmospheric cruise there is an MLI blanket in place that extends over the entire forebody and afterbody up to the spin-eject ring. There is no blanket over the spherical aft lid or the flat disk where the spin-eject ring mounts. The effective emissivity (ε^*) of the blanket, driven by JPL heater power limits, is 0.03. The exterior of the MLI, and the non-insulated portions of the vehicle, radiate to deep space and absorb solar fluxes as determined by their optical properties. The solar orientation during the four-day cruise varies from 45.2 degrees off the nose at separation to 47.5 degrees off the nose at entry.

The entry phase model includes the heat flux loads as discussed above. It also includes radiation between parts and radiation to the atmosphere. The atmospheric temperature as a function of time was derived from the altitude using a GRAM-95 model. Convection cooling to the atmosphere after the heat pulse will be added as a refinement later in the modeling. Radiation to the atmosphere is the driver in decreasing EEV surface temperatures. It is assumed that the MLI breaks away rapidly (as designed), so the surface emissivity used (0.8) is for the TPS itself.

The post-landing model includes the initial temperature from the entry phase, as well as radiation and convection to a 25°C ambient. The 25°C ambient is considered conservative since the projected landing in October in Utah would yield a colder ambient than that. All assumptions are designed to be conservative in the sense of predicting the warmest possible OS temperature.

Material Properties

Material properties for the TPS materials were taken from the TPSX software[7], with some modifications by NASA Ames personnel. Carbon-carbon and other composite properties were from Langley reports.[8,9] Other material properties were from vendor literature, from the PATRAN Thermal materials database, and from independent calculations. All material properties with substantial temperature variation were input as tables versus temperature.

Initially the materials were modeled as isotropic, which is not a valid assumption for some of the fiber-based materials such as the carbon-carbon structure. For these orthotropic materials, through-thickness and in-plane conductivity properties were added. In general, the in-plane conductivity is appreciably higher than the through-thickness property due to the in-plane orientation of the fibers. Thus, this model refinement makes a substantial difference in the heat flow and overall thermal behavior.

The difficulty in adding the orthotropic properties is that the materials are not oriented in any constant axis of the model. On the forebody carbon-carbon spherical cap, for example, the direction of the through-thickness property is changing continuously in two directions of rotation. In PATRAN, the orientation of an orthotropic material is

defined by three Eulerian rotation angles about the x, y and z axes. Since the Eulerian rotation of the material is different at each point on most of these components, a spatial field was used to define these rotations. By making the spatial field a specific function of two spatial variables, the field could be defined as exactly the Eulerian rotation necessary to bring the material axes into the correct orientation at each position. Each field was written as an equation of the following form:

$$\phi = \sin^{-1}\left(\frac{Z}{R}\right) * \cos\left(\tan^{-1}\left(\frac{X}{Z}\right)\right) \tag{1}$$

where ϕ is the material rotation around the x-axis, R is the component radius at that point, and X and Z are the location in the x and z axes. This equation was modified for the conical parts, as well as for parts such as the lid where the curvature was inverted (concave rather than convex). Each of the curved orthotropic components had x-rotation and z-rotation defined in this manner (no rotation around y since it was the axis of symmetry). Changes due to refining the material properties in this way are shown in the results sections.

Transfer to Structural Analysis

Transfer of temperatures to the structural model was very straightforward in the exo-atmospheric case. A routine within PATRAN's thermal solver (patq) can interpolate temperatures from one model to another, provided the models have the same geometry, even if the meshes are entirely different. The structural model was constructed from the same Pro/Engineer geometry used for the thermal model and was meshed with solid elements. The structural model mesh includes only structurally significant material, with the remaining components as distributed masses. Temperatures from the thermal-to-structural interpolation were used to assess stress and deformation under the thermal gradients. For the entry case, two methods were used. One was the same as previously described. In the second method, the structural model used meters as the length unit, and used mainly shell elements since this is how final models will probably be done. In this case, the structural model was scaled to the same units to allow thermal interpolation, and fields were applied to shells rather than solids. The process for interpolating the temperatures onto the meter-scale shell model were as follows: scale structural model back to millimeters for temperature interpolation, rotate scaled FEM to align with thermal FEM, interpolate temperatures from thermal to structural model, and run thermal strain analysis using scaled, rotated shell FEM.

RESULTS

Exo-Atmospheric Phase Results

After separation from the spacecraft, the EEV comes to equilibrium within several hours, and there are no major changes until the vehicle has a substantial view of Earth (in the last hour). Thus, the thermal behavior is constant over a majority of the time. This being the case, this model was usually run as steady state in order to quickly evaluate the effect of different boundary conditions and materials. Once a set of materials and coatings were selected, this model was run as a transient to evaluate the real-time behavior.

The thermal response during exo-atmospheric cruise is almost completely driven by the orientation of the EEV with respect to the sun, and by the coatings and coverings on the exterior of the EEV. Currently, it is assumed that MLI will be needed on the exterior of the EEV in order to minimize the heater power needed while attached to the spacecraft. The drivers on selecting exterior properties were as follows. The OS must be kept at a reasonably low temperature, well below the limit of 50°C. The adhesive bondlines should all be kept above –80°C to maintain structural integrity. The beacon assembly, which is located within the wing foam, should be kept above –40°C. In order to facilitate flight testing, it is desired that most structural components be kept as near room temperature as possible. Several parametric cases were run on an earlier concept to determine an optimum set of exterior properties[2], which were used for this analysis. The MLI was assumed to have exterior properties of $\alpha/\varepsilon = 0.6/0.3$. The aft lid was assumed to have a high virgin emissivity of 0.88, and the spin eject ring was slightly lower at 0.58.

The results are shown in Figure 9. The gradient across the vehicle is mainly driven by the solar flux on the forebody and by the absence of heating or MLI on the aft body. However, all components are within acceptable thermal ranges. It is expected that a lower emissivity coating will be selected for the aft body, thus bringing up the aft body temperatures and decreasing the overall gradient. The incorporation of 3D orthotropic properties in the analysis

decreased the predicted gradient across the vehicle by roughly 35°C to its current value of 81°C. The structural effects due to this thermal gradient are shown on the structural model in Figure 10. These strains are well within the materials' capability.

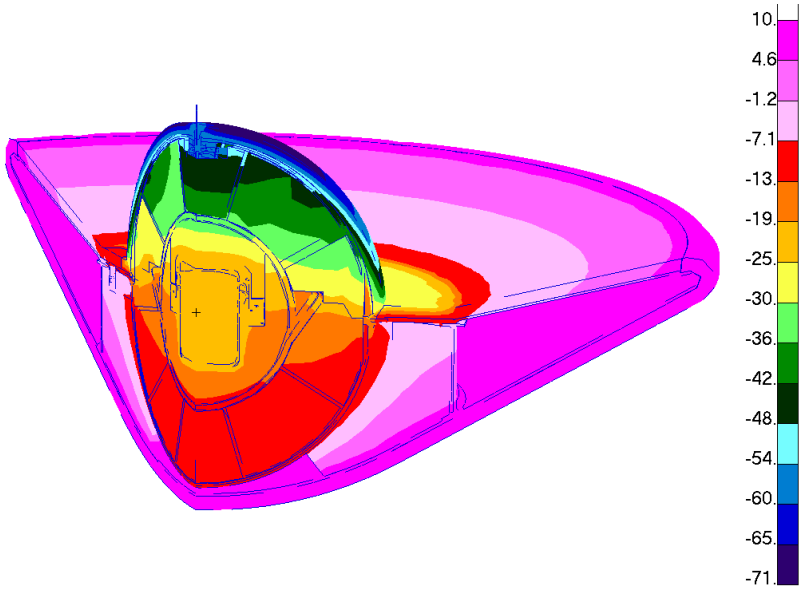

Figure 9. Exo-atmospheric temperature distribution (°C).

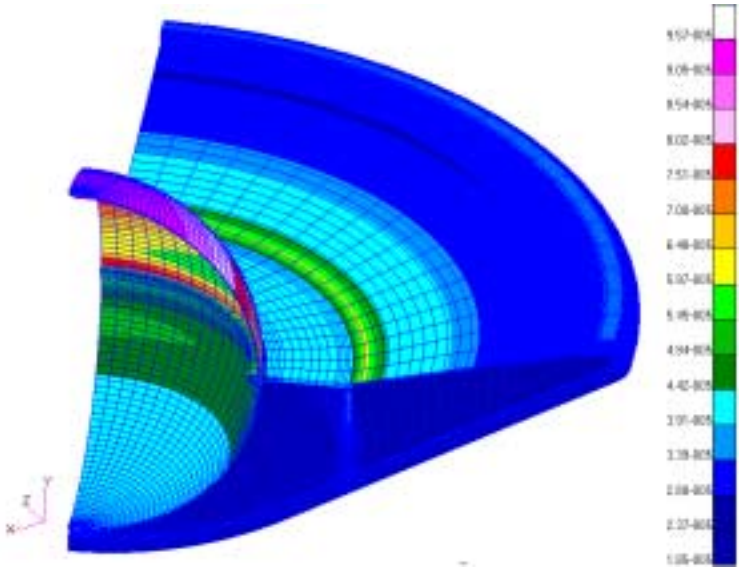

Figure 10. Structural model principal strain predictions based on temperature field.

Entry Phase Correlation to FIAT Model

The forebody and aftbody heating during entry dominate the thermal response of the EEV in this phase of the mission. Initial temperature predictions did not account for the energy loss due to charring and property change. The predicted temperature distribution at 45 seconds for this initial run without correlation is shown in Figure 11. Figure 12 shows the temperature history at the stagnation point through entry up to landing for both the PATRAN Thermal and FIAT models. At peak heating (17 seconds), a temperature difference of 149°C between the PATRAN and FIAT model occurred. At landing (360 seconds), there was a maximum temperature difference of 174°C. The temperature distribution at landing is shown in Figure 13. Obviously, neglecting the material charring has a substantial effect.

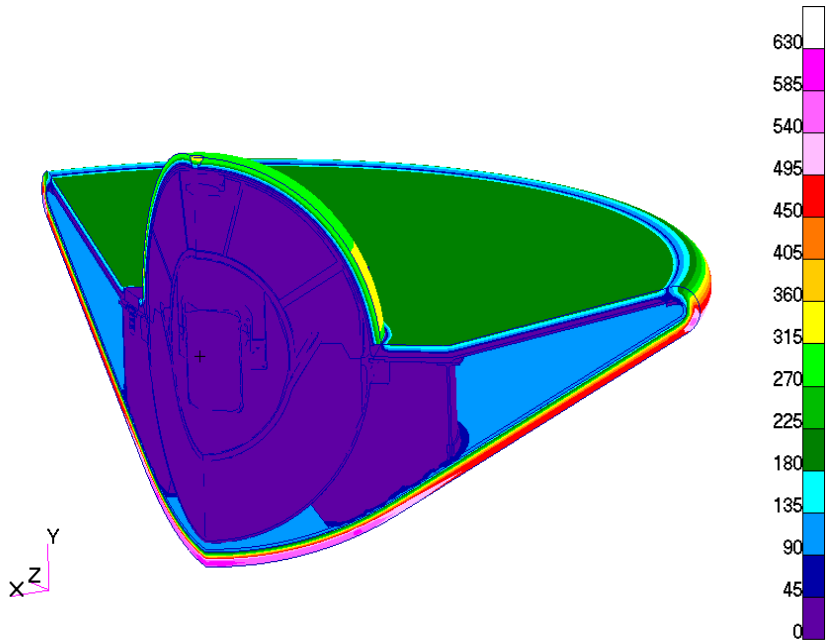

Figure 11. Entry temperature distribution at 45 sec (°C) -- uncorrelated.

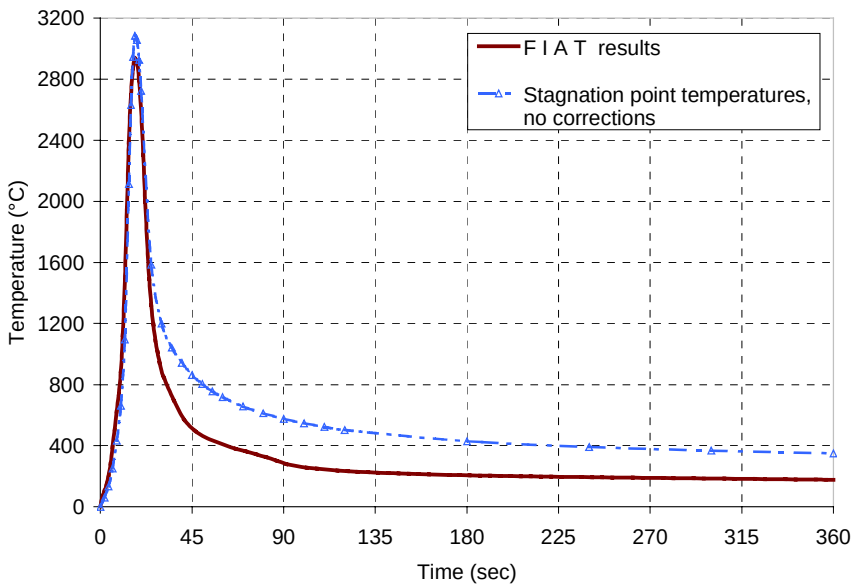

Figure 12. Stagnation point temperatures during entry for uncorrelated model.

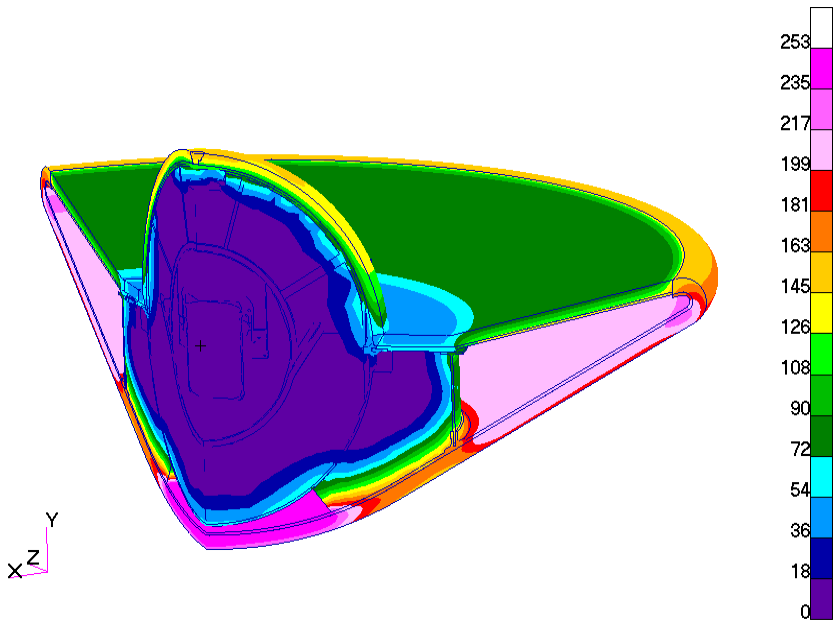

Figure 13. Entry temperature distribution at 360 sec (°C) -- uncorrelated.

These initial results showed unsatisfactory correlation largely due to the inability of PATRAN to directly model the ablative nature of the TPS material. In order to simulate the physical and chemical processes and achieve satisfactory correlation, an engineering adjustment to the PATRAN model was needed. Applying the hot wall heat flux from FIAT to the PATRAN model was an improvement from previous analyses in that it more closely approximated the actual heating on the vehicle, and thus a complex set of heat reduction functions were not needed. A time-varying reduction factor on the heat pulse was needed, however, to account for the energy lost due to mass loss. A peak reduction factor of 22.5% at 17 sec was all that was required to correlate the temperatures from 16 to 25 seconds. The form of the heat flux reduction, originally developed for a previous design configuration[2], was a simple sine function with time as the independent variable. This was used to smoothly transition from the baseline heating profile to the maximum reduction at peak heating in the following form:

$$Q_f = \left(A\sin^4 \omega t + B\sin^2 \omega t + C\sin\omega t + D\right) * Q_o \tag{2}$$

where t is time, Q_f is the corrected heat flux, Q_o is the FIAT hot-wall heat flux, and ω is the frequency of the sine function. The coefficients A, B, C, and D were determined by bounding the reduction factor between a given time interval, specifying the time the maximum occurs, and specifying the maximum value of the reduction factor. After 25 seconds, the effect of charring in changing the bulk material properties becomes significant enough to diverge the results. The FIAT code models charring directly such that the vehicle loses mass and hence loses some of its ability to store energy. Therefore, to simulate the loss of mass and energy in the PATRAN model, the first two layers of elements on the forward TPS were assigned material properties of charred carbon phenolic after 16 seconds (to average the time at which charring became significant). These two layers of elements were also given time-varying, decreasing density in order to simulate the loss of mass. With the combination of the heat reduction factor and the time varying char properties, the PATRAN results showed good correlation with the FIAT model. Figure 14 shows the correlation for the stagnation point, where the temperature difference is only 11.6°C at peak heating and 16.0°C at landing. A similar correlation was obtained for interior nodes in line with the stagnation point.

Slight adjustments to the aftbody heating were necessary to produce a satisfactory correlation at peak heating. A reduction factor of 20% when applied at 20 seconds to the aft body heating reduced the temperature difference from 96.3°C to 15.8°C. A charring approximation was not necessary as the PATRAN and FIAT models were in good agreement at landing where the temperature difference was 12.3°C. Figure 15 shows the temperatures at the stagnation point on the aft body. The reason for such close correlation without any major corrections was that the aftbody TPS material, SLA-561V, was not exposed to heating rates high enough to cause significant charring.

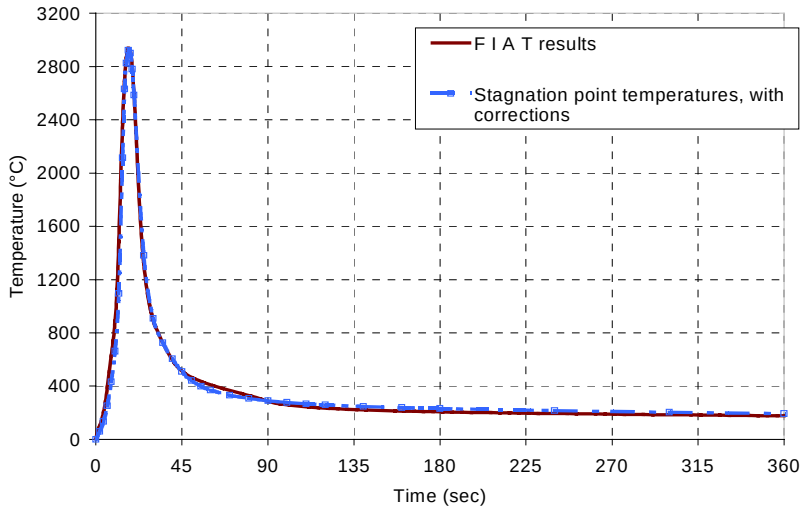

Figure 14. Correlated stagnation temperatures.

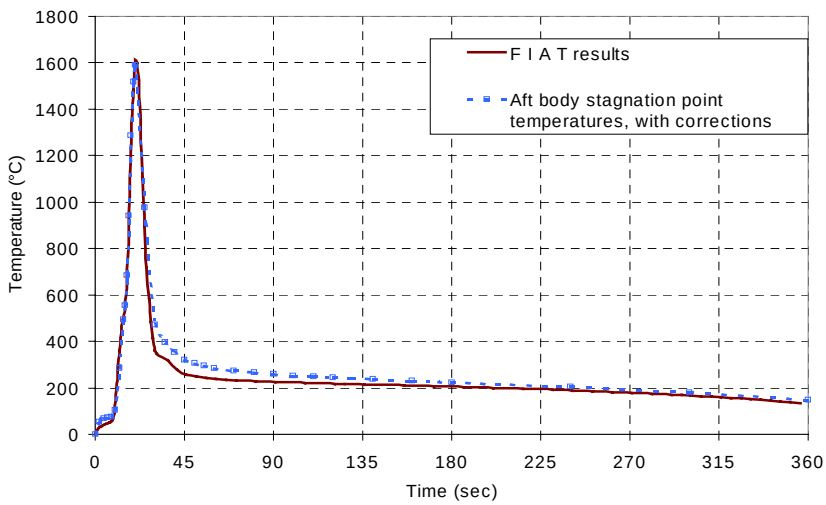

Figure 15. Correlated aft body stagnation temperatures.

Entry Phase Results

The prediction for Earth entry used these engineering adjustments, adds the refinement of 3D orthotropic properties, and included the initial temperatures from the exo-atmospheric phase of the mission. The results are shown in Figure 16 and Figure 17. The addition of the orthotropic properties increased the conduction through the energy absorbing core web material, which is directed towards the center of the energy-absorbing core. The effect of the orthotropic properties can also be seen in the forward TPS and structure, where the higher in-plane conductivity of the structure helped to evenly distribute the energy across itself and the TPS. Including the orthotropic properties decreased the temperature at the stagnation point, increased the temperature near the body foam and decreased the temperature in the shoulder region. The 3D orthotropic model was also analyzed starting at 0°C to allow direct comparison with the correlation runs that used a global initial temperature of 0°C. This verified that the orthotropic nature of the material, and not the initial temperature, caused the changes in thermal distribution. Figure 18 shows the temperature distribution at landing for this case, and shows the same trends are present as in the case with the initial temperatures from the exo-atmospheric phase.

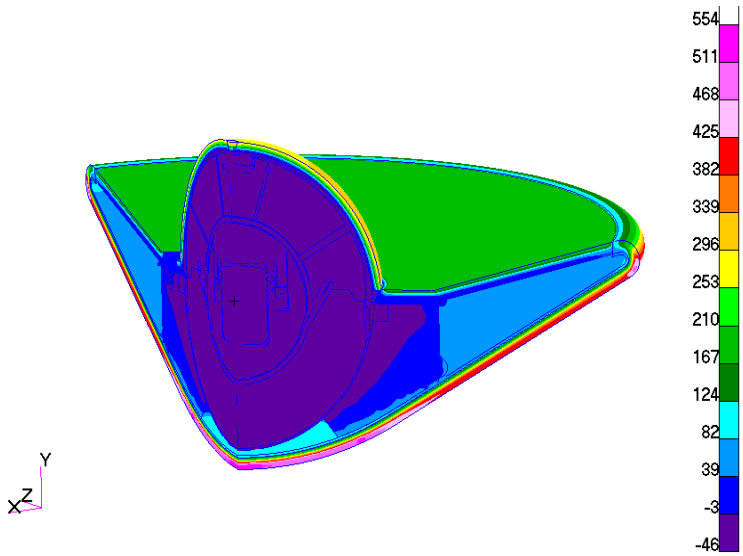

Figure 16. Entry phase temperature prediction at 45 s (°C).

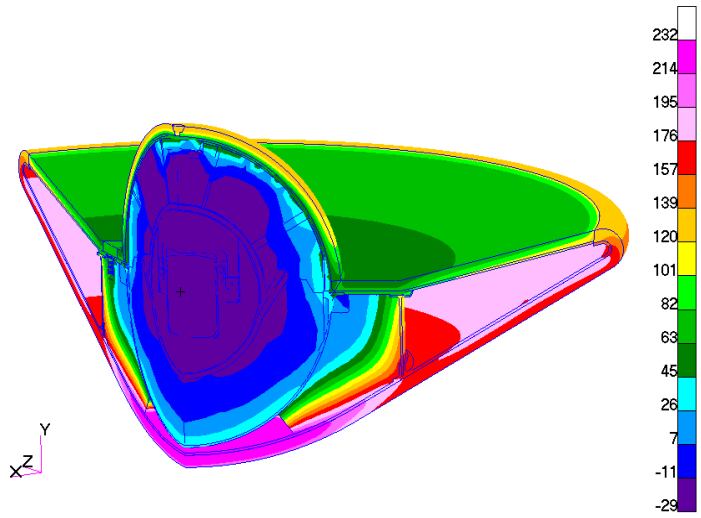

Figure 17. Entry phase temperature prediction at 360 s (°C).

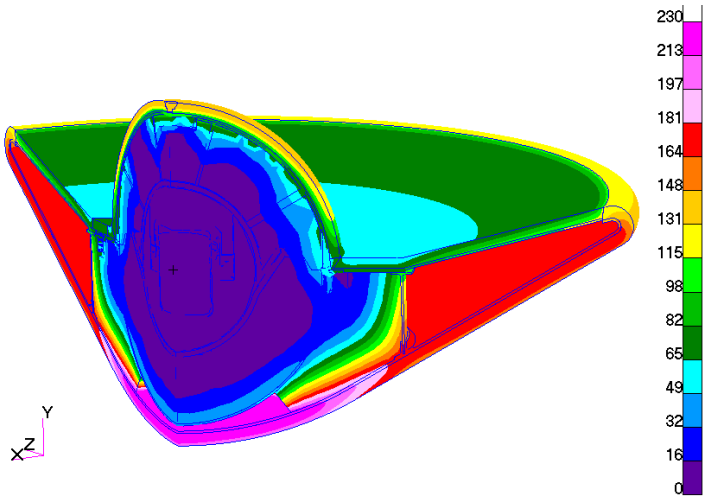

Figure 18. Entry phase temperature prediction at 360s (with 0°C initial temperature).

The structural predictions for the entry phase are shown in Figure 19 for the direct transfer to a solid model, and in Figure 20 for the interpolation to a shell model that used meters as the unit. These results are for the maximum pressure point in the trajectory, when the stresses on the material would be maximized. The interpolations give very similar results, except that in the shell model, thermal gradients across solids are not captured so some stresses are neglected. Strains are shown rather than stresses since these can be directly compared between solid and shell models. The strains are well within the capability of the carbon-carbon structural material. The pressure loads due to entry deceleration have not yet been combined with the thermal effects, but this is a relatively simple operation.

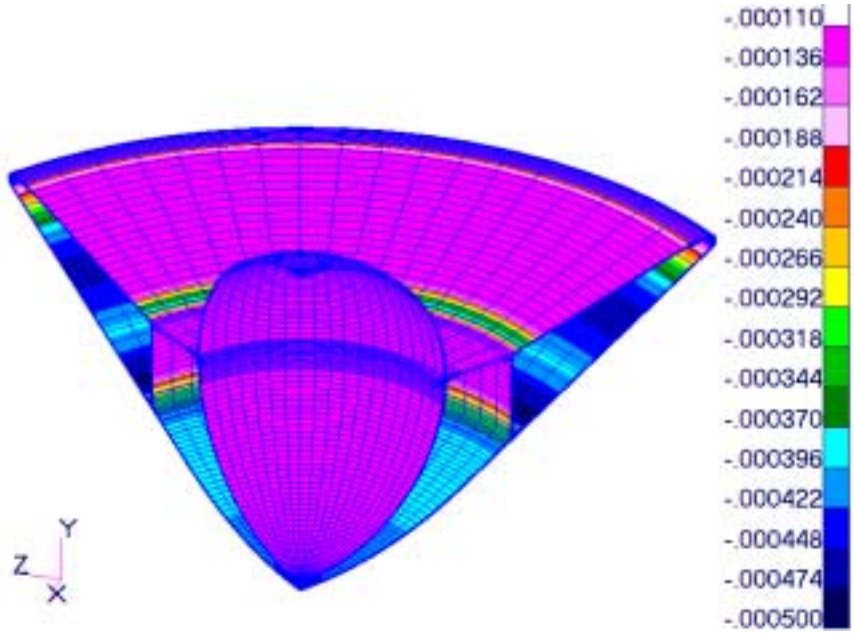

Figure 19. Strains for maximum pressure point at entry using solid model.

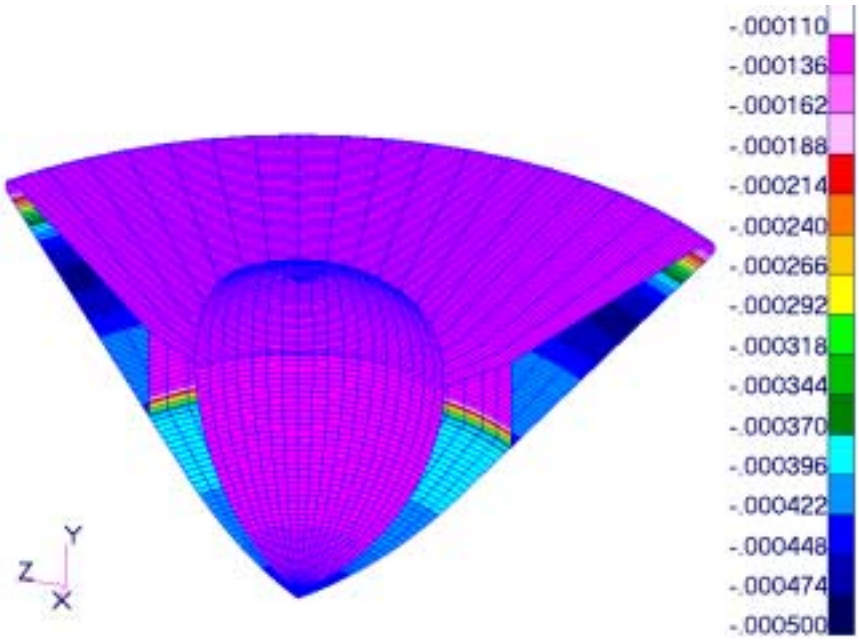

Figure 20. Strains for maximum pressure point at entry using shell model.

Landed Phase Results

After landing, the vehicle begins to come to thermal equilibrium. Figure 21 shows results of an example analysis of the progression. By four hours after landing, the vehicle is close to thermal equilibrium and few changes are occurring. At no time does the OS exceed the ambient temperature of 25°C. No combination of assumptions such as convection to ambient and which parts of the vehicle come in contact with the ground raise the OS temperature above 25°C.

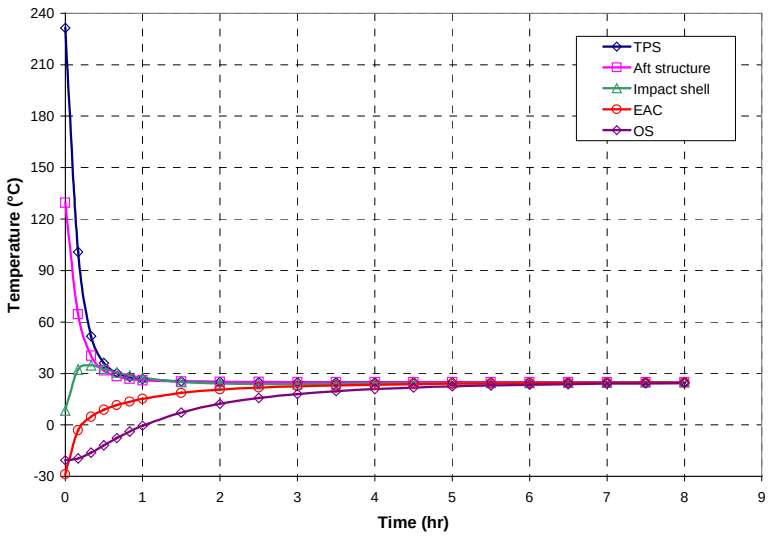

Figure 21. Transient after landing (°C).

CONCLUSIONS

A procedure was developed to perform detailed thermal analysis early in the design phase of the EEV for the Mars Sample Return mission. Results from this procedure indicate the passive design EEV was successful in maintaining all parts within their designed thermal limits. The thermal analysis was successfully coupled with the CAD design tool, aeroheating and material response analysis, orbital radiation analysis and structural analysis. While some improvements in the integration are planned, the current implementation linking the processes was of immense benefit in producing an accurate prediction of the EEV behavior. Orthotropic material properties were successfully added to all models using complex spatial fields, and produced meaningful changes in the predicted gradients.

ACKNOWLEDGEMENTS

The work of YK Chen at NASA Ames in analyzing the material response during entry, which allowed correlation of this analysis, is acknowledged with deep gratitude. The work of Stephen Hughes and Robert Dillman at NASA Langley in preparing CAD models is greatly appreciated.

ACRONYMS

CAD	Computer-aided design
CV	Containment vessel
EEV	Earth Entry Vehicle
FIAT	Fully Implicit Ablation and Thermal Analysis Program
MLI	Multi-layer insulation

OS	Orbiting samples
POST	Program to Optimize Simulated Trajectories
STEP	Standard for the Exchange of Product Model Data
TSS	Thermal Synthesizer System
TPS	Thermal protection system

REFERENCES

[1] R. A. Mitcheltree, S. Kellas, J. T. Dorsey, P. N. Desai and C. J. Martin, Jr., "A Passive Earth-Entry Capsule for Mars Sample Return," 7th AIAA/ASME Joint Thermodynamics and Heat Transfer Conference, Albuquerque, New Mexico, AIAA 98-2851, June 15-18, 1998.

[2] R. M. Amundsen, J. A. Dec, R. A. Mitcheltree, M. C. Lindell and R. A. Dillman, "Preliminary Thermal Analysis of a Mars Earth Entry Vehicle," 34th AIAA Thermophysics Conference, Denver, Colorado, June 19-22, 2000.

[3] Pro/ENGINEER Fundamentals Manual, Parametric Technology Corporation, Release 20.0 (June 1998).

[4] MSC/PATRAN User Manual, MacNeal-Schwendler Corporation, Version 9.0 (May 1999).

[5] User Manual, Thermal Synthesizer System, Release 6.01, Lockheed Martin Space Mission Systems, NAS9-19100, October 1997.

[6] Y. K. Chen and F. S. Milos, "Ablation and Thermal Response Program for Spacecraft Heatshield Analysis," *Journal of Spacecraft and Rockets*, Vol. 36, No. 3, 1999, pp. 475-482.

[7] TPSX, Thermal Protection Systems Expert and Material Properties Database, February 1998, NASA Ames Research Center (http://asm.arc.nasa.gov/tpsx/).

[8] C. W. Ohlhorst, W. L. Vaughn, P. O. Ransone, H. Tsou, "Thermal Conductivity Database of Various Structural Carbon-Carbon Composite Materials," NASA TM-4787, NASA Langley Research Center, November 1997.

[9] E. M. Silverman, "Composite Spacecraft Structures Design Guide," NASA Contractor Report 4708, Contract NAS1-19319, March 1996.